Indian Journal of Chemistry
Vol. 57A, January 2018, pp. 44-51

Crystal structure, configurational and DFT study of nickel(II) complexes with N_2O-donor type Schiff base ligand

Yogendra Pratap Singh, Ram N Patel* & Yogendra Singh

Department of Chemistry, APS University, Rewa (MP) 486 003, India

Email: rnp64@ymail.com

Received 11 February 2017; revised and accepted 20 December 2017

Nickel(II) complexes containing a Schiff base (L) derived from 2-pyridinecarboxyldehyde and 2-furoic hydrazide $[Ni(HL)(L)]NO_3$ (**1**) and $[Ni(L)_2]4H_2O$ (**2**) where HL = *N*'-[(*E*)-pyridin-2-yl-methylidene]furan-2-carbohydrazide, have been synthesized and comprehensively characterized via physico-chemical techniques as well as by single crystal X-ray structural analysis. In both the complexes, the ligand behaves as mono-anionic tridentate and binds to the nickel(II) ion via deprotonated carbonyl-oxygen, pyridine-nitrogen and azomethine-nitrogen. Magnetic moments and electronic studies suggest an octahedral geometry around nickel(II) ion in both the complexes. The supramolecular architecture in both (**1**) and (**2**) are shown by C-H...π and π…π interactions. The molecular structures and spectral properties of the complexes have been explained by DFT and TD-DFT calculations. The electronic excitation energies of these complexes, calculated at TD-DFT levels, are in agreement with values deduced from the experimental UV-visible spectra.

Keywords: Coordination chemistry, Supramolecular architecture, X-ray structures, π…π interactions, C-H…π interactions, UV-visible spectroscopy, TD-DFT calculations, Schiff bases, Nickel

The coordination chemistry of Schiff base transition metal complexes have been studies extensively due to the synthetic flexibilities of Schiff base ligands and their selectivity as well as sensitivity towards the metal ions. For long, considerable attention has been paid to the chemistry of the metal complexes of Schiff-base containing nitrogen and other donors and it has become an emerging area of research[1]. Nickel(II) has a very fascinating coordination chemistry owing to its inherent ability to adopt various geometries, which often interconvert and such a configurational switch is generally associated with color change.

Synthesis and structural investigation for a series of nickel(II) octahedral complexes have been reported[2] and these have achieved success in generating stable nickel(II) complexes Xu *et al*.[3] have studied the coordination mode of aryl-hydrazone and their metal complexes. The most commonly used approach for engineering the crystal structures of such systems is to employ their hydrogen bonds[4]. The quantum chemical studies carried out using the density functional theory (DFT) calculations have become an increasingly useful tool for predicting the geometry and harmonic vibration of organic compounds[5,6]. The success of DFT is mainly due to the fact that it describes the small molecules more reliably. It is a useful method for investigation of large molecules as well[7]. To show the existence of intramolecular charge transfer (ICT) within molecular systems, energies of the highest occupied molecular orbital (HOMO) and lowest unoccupied molecular orbital (LUMO) levels and the molecular electrostatic surface potential (MESP) energy surface studies have been carried out by DFT[8]. Herein, we present the synthesis and characterization of Schiff base ligand HL and two mononuclear nickel(II) complexes. XRD structures have been determined by single crystal X-ray analysis. DFT calculations are also performed to support the experimental results.

Materials and Methods

Nickel(II) nitrate hexahydrate, nickel(II) perchlorate hexahydrate, 2-pyridinecarboxaldehyde and 2-furoic hydrazide were obtained from commercial sources and used without any further purification. All other chemicals were of synthetic grade and used as received. Schiff base was prepared by standard literature procedure[3,9] and recrystallized from ethanol.

The ligand, HL, was synthesized by refluxing 2-pyridin-carboxyldehylde (0.951 g, 10 mmol) was reacted with 2-furoic hydrazide (1.261 g, 10 mmol).

The resulting light yellow solution was stirred for 4 h at 75 ºC. After evaporation of the solvent, a light yellow solid was obtained. Yield: 80%. Anal. (%): Found: C, 61.41; H, 4.21; N, 19.57. Calcd: C, 61.39; H, 4.22; N, 19.53; O, 14.87.

Synthesis and characterisation of (1) and (2)

$[Ni(HL)(L)].NO_3$. (**1**): To a methanol (20 mL) solution of $[Ni(NO_3)_2]6H_2O$ (0.290 g, 1 mmol), was added a (20 mL) solution of HL (0.430 g, 2 mmol) drop-wise. The resulting blue solution was stirred at room temperature for 30 min. Single crystals of (**1**), suitable for X-ray structure determination, were obtained by slow evaporation of the filtrate over a week. Anal. (%): Found for $C_{22}H_{17}N_6NiO_7$: C, 47.95; H, 2.95; N, 17.79. calcd: C, 47.89; H, 3.01; N, 17.81. FAB mass (*m*/*z*): Found (calcd) 488.12 (488.10). IR (KBr) cm^{-1}: υ(C=N) 1588, υ(-N-H) 3120, υ(C=O) 1619, free NO_3 1437, 1317, 860, υ(Ni-O) 424 and υ(Ni-N) 410 cm^{-1} (Supplementary Data, Fig. S1).

$[Ni(L)_2]4H_2O$ (**2**) was synthesized by a procedure similar to that used for (**1**) except that nickel perchlorate was used instead of nickel nitrate. The colour of the reaction mixture was deep blue. Anal. (%): Found for $C_{22}H_{24}N_6NiO_8$: C, 47.26; H, 4.33; N, 15.03. calcd: C, 47.30; H, 4.39; N, 15.21. FAB mass (*m*/*z*): Found (calcd) 487.08 (487.11). IR (KBr) cm^{-1}: υ(H_2O) 3427, υ(C=N) 1599, υ(Ni-O) 425 and υ(Ni-N) 416 cm^{-1} (Supplementary Data, Fig. S2).

Elemental analyses were performed on a Euro Vector EA3000 elemental analyzer. FAB mass spectra were recorded on Jeol SX 102/DA 6000 mass spectrometer using xenon (6 kV, 10 mA) as the FAB gas. The accelerating voltage was 10 kV and the spectra were recorded at RT with *m*-nitrobenzyl alcohol as the matrix. Infrared (IR) spectra were recorded on a Bruker spectrophotometer at normal temperature with KBr pellets by grinding the sample with KBr (IR grade), in the range of 400-4000 cm^{-1}. Electronic absorption spectra (300-1100 nm) were recorded in solution on a Shimadzu UV-vis spectrophotometer (UV-1601). RT magnetic susceptibilities were measured on a Gouy balance using a mercury(II) tetrathiocyanato cobaltate(II) as calibrating agent (χ_g = 16.44×10^{-6} cgs units). Diamagnetic corrections were estimated from Pascal tables. Effective magnetic moments were calculated using the equation, $\mu_{eff} = 2.83(\chi_M T)^{1/2}$, where χ_M is the molar magnetic susceptibility. Molar conductances were measured using a Systronic, conductivity-TDS meter-308.

X-ray studies

X-ray quality single crystals were obtained by slow cooling of methanol solutions of (**1**) and (**2**). Crystallographic analysis was carried out with a Bruker Apex-II diffractometer for (**1**) and (**2**). Graphite monochromated Cu-Kα radiation (λ = 1.54182 Å) was used, all operating at 50 kV and 30 mA. Intensity data were collected at 298 K for (**1**) and (**2**), using the ω-2θ scan technique. Cell refinement, indexing and scaling for the data set were carried out using the Bruker Saint packages[10]. Structures were solved by direct methods and subsequent Fourier analyses[11] and refined by the full-matrix least square method based on F^2 with all observed reflections[11] with absorption correction applied using SADABS[12]. All structures were solved by direct methods using the SHELXS package[13] and refined with SHELXL-2014[13]. All the non-hydrogen atoms were refined anisotropically and all the hydrogen atoms were fixed by HFIX and placed in ideal positions. All calculations were performed using the SHELXL97, PLATON and WinGx (ver. 1.80.05) systems[14].

In complex (**1**), the entire structure was disordered over two positions at half occupancy with an oxygen atom. In (**2**), a water molecule was in more than one occupancy sharing in the lattice. SQUEEZE[15] was used to correct potential value of 2662.1 and 2569.7 $Å^3$ for (**1**) and (**2**), respectively. The refinement with (without) the model treatment gives R values of 0.0567 (0.1574) and 0.1150 and 0.3135 for (**1**) and (**2**)**,** respectively, thus improving this parameter by 60%. Crystallographic data are summarized in Table 1.

Theoretical studies

The entire theoretical calculations of complexes were performed at DFT level employing Becke's three parameters hybrid exchange functional and the Leee Yange Parr correlation functional (B3LYP)[16] using the 6-31G & LANL2DZ basis set with the help of Gaussian09 and Gauss view 5.0 softwares[17]. The molecular geometries of all the compounds were optimized in gas phase using B3LYP/6-31G and B3LYP/LANL2DZ basis set and no symmetry restrains were applied. Optimized structural parameters were used to evaluate the HOMO-LUMO energy and spin densities[18].

Results and Discussion

The nickel(II) complexes were obtained by the direct reaction of the HL ligands with $Ni(NO_3)_2{\cdot}6H_2O$

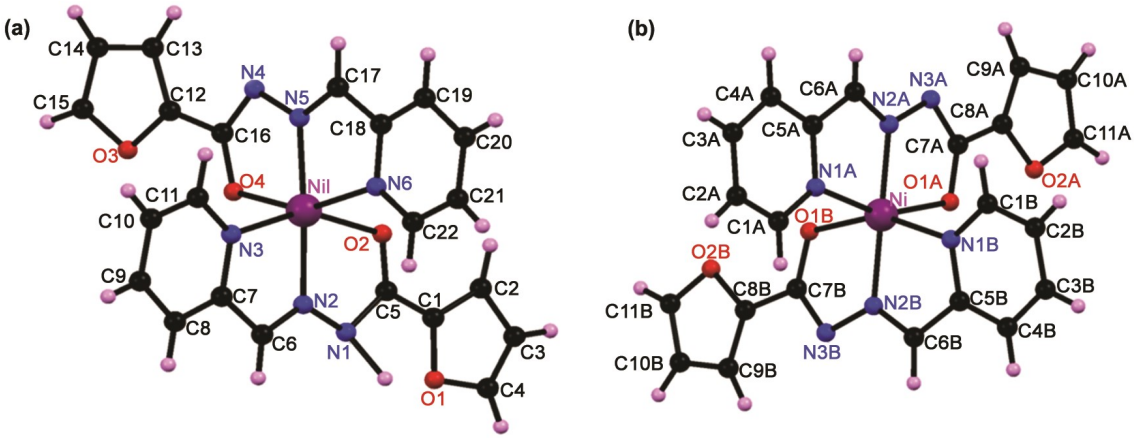

Fig. 1 — Crystal structure with atomic numbering scheme of (a) $[Ni(HL)(L)]^+$ (**1**) and (b) $[Ni(L)_2]$ (**2**).

and $Ni(ClO_4)_2 \cdot 6H_2O$ in methanol in a 2:1 ratio. Both complexes are soluble in DMSO, DMF, acetonitrile, ethanol and methanol, and are insoluble in diethyl ether. These complexes are stable in air. Both complexes were characterized using elemental analysis and further characterized by FAB^+ mass spectrometry. The μ_{eff} values (2.79 BM for (**1**) and 2.82 BM for (**2**)) observed for complexes, correspond to two unpaired electrons and suggest a high-spin octahedral geometry for the complexes. The molar conductivities (λ_m) of DMSO solutions (3.0×10^{-3} mol L^{-1}) of complexes (**1**) and (**2**) were measured. The value of 110 Ω^{-1} cm^2 mol^{-1} for (**1**) indicates it is a 1:1 electrolyte[19], whole, the value λ_m = 13 Ω^{-1} cm^2 mol^{-1} for complex (**2**) suggests it is a non-electrolyte[20].

The molecular structures of complexes (**1**) and (**2**) are shown in Fig. 1(a & b). Crystal data and structural refinement parameters of the complexes are presented in Table 1. Selected bond distances and angles are collected in Table 2. The nickel(II) centers are in a distorted octahedral geometry with a N_4O_2 donor environment. The distortions from ideal octahedral geometry about Ni(II) are to the same extent as those commonly observed for nickel(II) complexes containing multidentate ligands[21]. Individual mean distances and angles compare well with those found for other octahedral nickel(II) complexes involving nitrogen donors[22].

X-ray studies

Complex (**1**) crystallizes in the monoclinic space group $P2_1/c$ with four molecules in the unit cell. Nickel is in a distorted axially compressed octahedron (Table 2). The ligand is tridentate via one pyridyl nitrogen, one hydrazone nitrogen and one carbonyl

Table 1 — Crystallographic data and structure refinements of complexes (**1**) and (**2**)

	(**1**)	(**2**)
Emp. formula	$C_{22}H_{17}N_6NiO_4$	$C_{22}H_{24}N_6NiO_8$
Formula wt	488.12	559.16
T (K)	298(2)	298(2)
λ (Å)	1.54184	1.54184
Crystal system	Monoclinic	Monoclinic
Space group	$P2_1/c$	$P2_1/n$
Unit cell dimensions		
a (Å)	14.1894(6)	10.3428(2)
b (Å)	8.5335(4)	22.7047(5)
c (Å)	22.0165(11)	10.9547(2)
α (°)	90	90
β (°)	93.050(5)	92.682(2)
γ (°)	90	90
Vol. ($Å^3$)	2662.1(2)	2569.68(9)
Z	4	4
Density (calc.) (mg/m^3)	1.218	1.492
Abs. coeff. (mm^{-1})	1.353	1.549
Crystal size (mm^3)	0.15×0.28×0.19	0.22×0.17×0.11
θ (°)	3.119 to 71.955	3.894 to 71.823
Index ranges	$-17 \le h \le 16$, $-10 \le k \le 6$, $-23 \le l \le 26$	$-11 \le h \le 12$, $-26 \le k \le 27$, $-8 \le l \le 13$
Refl. collected	10339	10984
Data/restraints/parameters	5074/0/302	0.8322 and 0.7232
Goodness-of-fit on F^2	1.037	1.031
Final *R* indices [I>2sigma(I)]	*R1* = 0.0567, w*R2* = 0.1574	*R1* = 0.1150 w*R2* = 0.3135
R indices (all data)	*R1* = 0.0746, w*R2* = 0.1765	*R1* = 0.1220 w*R2* = 0.3211

Table 2 — Coordination bond length (Å) and angles (°) for (**1**) and (**2**)

$[Ni(HL)(L)]NO_3$ (**1**)					
	X-ray	DFT		X-ray	DFT
Ni(1)-N(5)	1.978(2)	1.989	Ni(1)-N(2)	2.005(2)	2.123
Ni(1)-O(4)	2.080(2)	2.321	Ni(1)-N(3)	2.081(2)	2.156
Ni(1)-N(6)	2.120(3)	2.345	Ni(1)-O(2)	2.200(2)	2.245
N(1)-N(2)	1.365(4)	1.352	N(1)-C(5)	1.348(4)	1.325
N(4)-N(5)	1.367(3)	1.374	N(4)-C(16)	1.337(4)	1.346
N(5)-Ni(1)-N(2)	175.65(10)	175.78	N(5)-Ni(1)-O(4)	77.17(9)	77.43
N(2)-Ni(1)-O(4)	98.49(10)	98.79	N(5)-Ni(1)-N(3)	102.60(10)	102.98
N(2)-Ni(1)-N(3)	77.72(10)	78.01	O(4)-Ni(1)-N(3)	94.57(9)	94.76
N(5)-Ni(1)-N(6)	78.31(10)	78.92	N(2)-Ni(1)-N(6)	106.03(10)	106.12
O(4)-Ni(1)-N(6)	155.43(9)	155.69	N(3)-Ni(1)-N(6)	92.11(9)	92.91
N(5)-Ni(1)-O(2)	104.68(9)	104.79	N(2)-Ni(1)-O(2)	75.12(9)	75.97
O(4)-Ni(1)-O(2)	92.05(8)	92.91	N(3)-Ni(1)-O(2)	152.71(9)	152.89
N(6)-Ni(1)-O(2)	92.77(9)	92.98			
$[Ni(L)_2]4H_2O$ (**2**)					
Ni-N(2A)	1.967(5)	2.012	Ni-N(2B)	1.980(5)	2.031
Ni-O(1B)	2.092(4)	2.189	Ni-N(1A)	2.094(5)	2.123
Ni-N(1B)	2.104(5)	2.431	Ni-O(1A)	2.116(4)	2.326
N(2A)-Ni-N(2B)	176.87(19)	176.92	N(2A)-Ni-O(1B)	100.97(17)	101.23
N(2B)-Ni-O(1B)	76.87(17)	76.98	N(2A)-Ni-N(1A)	78.97(19)	79.01
N(2B)-Ni-N(1A)	103.26(19)	103.35	O(1B)-Ni-N(1A)	91.57(17)	91.96
N(2A)-Ni-N(1B)	103.41(18)	103.76	N(2B)-Ni-N(1B)	78.71(18)	78.94
O(1B)-Ni-N(1B)	155.58(18)	155.87	N(1A)-Ni-N(1B)	94.48(18)	95.01
N(2A)-Ni-O(1A)	76.57(17)	76.87	N(2B)-Ni-O(1A)	101.18(17)	101.35
O(1B)-Ni-O(1A)	92.98(16)	93.04	N(1A)-Ni-O(1A)	155.54(18)	155.91
N(1B)-Ni-O(1A)	91.23(17)	91.98			

oxygen, thus forming bis chelated having four fused five-membered rings. The ligand is coordinated meridionally and would be perpendicular in an idealized octahedron. The ligand is deprotonated in the presence of metal ion and forms a complex with the metal in neutral media. Protonated ligand can also undergo similar reaction with metals. Complex (**1**) contains one poorly disordered nitrate. An interesting feature of this complex is that one N–H proton of one ligand is protonated which allows the charge on the complex to be balanced. The apical position is occupied by pyridine nitrogen (N6) with carbonyl oxygen (O4) completing the octahedral coordination sphere. The basal plane comprises the atoms N(5), O(2), N(2) and N(3). Sum of the basal angles [N(5)-Ni(1)-O(2) = 104.43º, N(5)-Ni(1)-N(3) = 102.60º, N(2)-Ni(1)-N(3) = 77.72º, N(2)-Ni(1)-O(2) = 75.12º] is 360º. In **1**, the C–N bond length N(4)–C(16) =1.337(4) Å is of double-bond character and the N(1)–C(5) =1.348(4) Å of single-bond character. At the same time, the N-N bond length is also reduced in L. These factors confirm the coordination through the enolate form by deprotonation after enolization of the ligand while one N–H proton of one ligand is protonated by coordination through the ketonic form of the ligand. The distortion of the molecule is indicated by the decreased value of the *trans* angles, N(5)–Ni(1)–N(2) = 175.65(10)°, N(3)–Ni(1)–O(2) = 152.71(9)° and O(4)–Ni(1)–N(6) = 155.43(9)°. Bond distances around the metal are Ni(1)–N(5) = 1.978(2) Å, Ni(1)–N(2) = 2.005(2) Å, Ni(1)–O(2) = 2.200(2) Å, Ni(1)–O(4) = 2.080(2) Å, Ni(1)–N(3) = 2.081(2) Å and Ni(1)–N(6) = 2.120(3) Å. The shorter Ni-N(2A) bond distance as compared to Ni-N(1A) suggests that the azomethine nitrogen coordinates more strongly than the pyridyl nitrogen[23]. Individual bond distances and angles within the coordination polyhedron compare well with those found in other octahedral complexes of nickel(II) involving N-donors[21,22]. The *cis* and *trans* angles reflect the degree of distortion from ideal octahedral geometry. The nickel atom is displaced by 0.025 Å from the planes constituted from

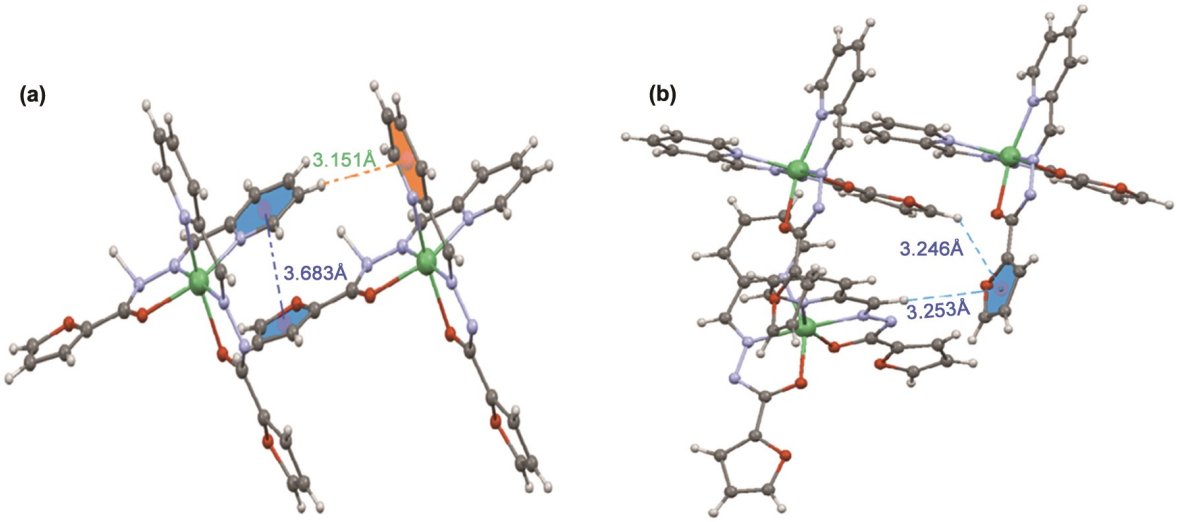

Fig. 2 — 3D supramolecular structure of complexes (a) C-H…π and π…π interactions of $[Ni(HL)(L)]^+$ (**1**) and (b) C-H…π interactions of $[Ni(L)_2]4H_2O$ (**2**).

the atoms C1, C2, C3, C4, O1,C5, N1, N2, C6, C7, C8, C9, C10, C11, N3 and N5.

The hydrogen atom H(10A), attached to C(22), is involved in intermolecular C-H…π interaction with symmetry (-*x*,1/2+*y*,1/2-*z*) related phenyl ring, C(18)-C(19)-C(20)-C(21)-C(22)-N(6), to form a one-dimensional supramolecular chain (Fig. 2a). The C-H…π distance is 3.151 Å with an angle 164.84º. In the crystal structure of (**1**), π…π interactions are also observed between the aromatic moieties of the pyridine π e^- and π e^- of furan ring (Fig. 2a). These π…π interactions between coordinated pyridine rings are defined by the atoms C(7)-C(8)-C(9)-C(10)-C(11)-N(3) interacting with furan π electron of C(1)-C(2)-C(3)-C(4)-O(1) (3.683 Å).

Complex (**2**) also crystallizes in the monoclinic space group $P2_1/n$. The two tridentate ligand (L) are coordinated with nickel(II), similar to that in (**1**). The coordination environment around nickel(II) is a distorted octahedral N_4O_2 geometry (Fig. 1b). The structure has a highly distorted octahedron with four crystalline lattice water. The distortion of the molecule is indicated by the decreased value of the *trans* angles, N(2A)–Ni–N(2B) = 176.87(19)°, N(1A)–Ni–O(1A) = 155.54(18)° and O(1B)–Ni–N(1B) = 155.58(18)°. Bond distances around the nickel(II) are Ni–N(2a) = 1.967(2) Å, Ni–N(2B) = 1.980(5) Å, Ni–O(1B) = 2.092(4) Å, Ni–O(1A) = 2.116(4) Å, Ni–N(1A) = 2.094(5) Å and Ni–N(1B) = 2.104(5) Å. In this complex also, the azomethine nitrogen coordinates more strongly than the pyridyl nitrogen[20]. Bond distances around nickel(II) are given in Table 2. The values obtained for this complex are comparable with the literature values for similar nickel(II) complexes[21,22]. The nickel resides in a distorted octahedral environment. The distortion can be further evidenced from the deviation of the *cisoid* and *transoid* angles from the ideal values Table 2.

The complex molecules are interconnected through the two C-H…π interactions in the crystal structure. The hydrogen atom, H(11A), attached to C(9A) and C(8A), are involved in C-H…π interaction with the symmetry (1/2+*x*,1/2-*y*,1/2+*z*) related furan ring, C(8A)-C(9A)-C(10A)-(C11A)-O(2A) with another hydrogen atom, H(6B), attached to C(11A), involved in the C-H…π interaction with the symmetry (1/2-*x*,1/2+*y*,1/2-*z*), related to same furan ring, to form a three-dimensional supramolecular network, as shown in Fig. 2(b). The C-H…π bond lengths are 3.246 Å, 3.253 Å and angles 129.67º for C(11B)-H(11B)…π and 157.14º for C(6B)-H(6B)…π, respectively.

Spectral studies

The degree of structural distortion from ideal octahedral geometry can be described through a tetragonality parameter (*T*), defined as $T = R_{int}/R_{out}$, where R_{int} and R_{out} are the average in-plane and out-of-plane distances, respectively. The nature of Jahn-Teller distortion is decided by the calculated *T* values of complexes (**1**) and (**2**)**.** This parameter shows static ($T < 0.9$) and dynamic ($T = 1$) distortions[24]. For complexes (**1**) and (**2**), *T* values (0.990 for (**1**) and 0.941 for (**2**)) show a dynamic Jahn-Teller distortion.

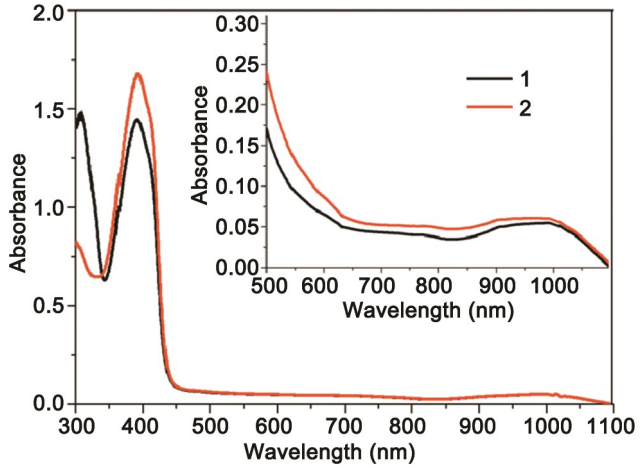

Fig. 3 — UV-visible spectra of complexes (**1**) and (**2**) (0.00025 mol dm^{-3}). [Inset: UV-visible spectra of complexes (**1**) and (**2**) (0.003 mol dm^{-3})].

The RT electronic spectra of (**1**) and (**2**) recorded in DMSO show three absorptions ($^3A_{2g}\rightarrow{}^3T_{2g}(\upsilon_1)$, $^3A_{2g}\rightarrow{}^3T_{1g}(F)$ (υ_2), $^3A_{2g}\rightarrow{}^3T_{1g}(P)(\upsilon_3)$) (Fig. 3), characteristic of octahedral complexes[19,25-27]. Electronic spectra of the complexes in DMSO also show a shoulder at 790 nm. This band appears to be an overlapping of the spin-allowed transition with the spin-forbidden transition, $^3A_{2g}\rightarrow{}^3T_{1g}(P)$. The $^3A_{2g}\rightarrow{}^3T_{1g}(P)$ band, marked by the high-intensity charge transfer band around 380 nm. Additionally, there are charge-transfer bands and intra-ligand transition present in the UV region for both the complexes. The ligand-field parameter *D*q (1002 for (**1**) and (**2**)) lowest energy transition was in the range for octahedrally coordinated nickel(II)[28]. The experimentally observed absorption bands of the complexes have been explained with the help of TD-DFT calculations. The vertical excitation energies, oscillator strength and tentative nature of the transitions obtained at the TD-DFT level are presented in Table S1 (Supplementary Data). The absorption bands ~381 nm for complexes (**1**) and (**2**) are due to the HOMO→LUMO+2 electronic excitations and can be assigned to π–π* transitions. The calculated molecular orbital electronic transitions of (**1**) are shown in Fig. S3 (Supplementary Data).

The band at 998 nm for (**1**) appears to be a composition of two excitations at 0.698 eV (λ = 1229 nm and *f* = 0.00) and 1.011 eV (λ = 1036 nm and *f* = 0.0001), due to the contributions of HOMO-1→LUMO+1 (23%) and HOMO→LUMO (18%) transitions. These may be attributed to a combination of *dπ*(Ni)→*dπ**(Ni) transitions. Similarly, the band at 620 nm appears to be a composition of two excitations at 1.562 eV (λ = 628 nm and *f* = 0.0005) and 1.421 eV (λ = 761 nm and *f* = 0.0041), which may again be attributed to a combination of MLCT/*dπ*(Ni)→*dπ**(Ni) charge transfer transitions. The shoulder band at 790 nm (λ = 857 nm and *f* = 0.002) is due to HOMO-1→LUMO transition and can be assigned to a mixture of LMCT/MLCT/ *dπ*(Ni)→*dπ**(Ni) transition.

Similarly in complex (**2**), the absorption band at 998 nm appears to be a composition of two vertical excitation at 0.393 eV (λ = 1187 nm and *f* = 0.0005) and 1.0071 eV (λ = 1031 nm and *f* = 0.0002) due to the HOMO→LUMO (87%) and HOMO-1→LUMO+1 (51%) of β-spin state excitations. These may be assigned to the *dπ*(Ni)-*dπ**(Ni) transitions. Similarly, the band at 621 nm is a combination of two excitations at 1.427 eV (λ = 768 nm and *f* = 0.0003) and 1.663 eV (λ = 745 nm and *f* = 0.0003), which may be assigned to MLCT/*dπ*(Ni)-*dπ**(Ni) transitions. The shoulder band at 790 nm comprises one vertical excitation at 1.341 eV (λ = 824 nm and *f* = 0.0007) due to the HOMO→LUMO+2 (48%) of β-spin state transition (Fig. S4, Supplementary Data) which may be assigned to a mixture of MLCT/ *dπ*(Ni)-*dπ**(Ni) charge transfer transition.

DFT studies

The geometries of nickel(II) complexes (**1**) and (**2**) were fully optimized by the DFT/B3LYP method using Gaussian09 software (Fig. S5, Supplementary Data). The structural agreement has been verified on comparing the bond distances and angles between the DFT optimized and X-ray determined structures of complexes (**1**) and (**2**) (Table 2). According to Table 2, the optimized bond lengths and angles are slightly larger than the experimental ones since the theoretical calculations were performed on isolated molecules in gas phase, whereas the experimental results were obtained in solid state[29-31].

The energy gap between the HOMO-LUMO orbitals indicates the molecular chemical stability[32]. A large HOMO-LUMO gap indicates a stable molecule with low chemical reactivity[33]. The energy gap between the HOMO-LUMO is important to determine the electrical transport properties of molecules[34]. The HOMO is the orbital that primarily acts as an electron donor and LUMO is the orbital that largely acts as electron acceptor. The HOMO energy are –5.145 and –4.140 eV, while the LUMO energy is –2.156 and –2.198 eV for (**1**) and (**2**), respectively. The HOMO-

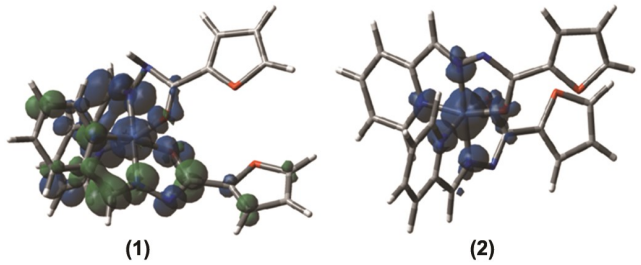

Fig. 4 — Spin density plots of complexes (**1**) and (**2**).

LUMO energy gaps are –2.989 eV for (**1**) and –1.942 eV for (**2**). The selected frontier molecular orbitals, energy level diagrams and their respective positive and negative regions of the complexes (**1**) and (**2**) are shown in Figs S3 and S4 (Supplementary Data), respectively. The lower value of HOMO-LUMO (ΔE) molecular orbital indicates that the molecule is more active. According to energy gap value, complex (**1**) is more active than (**2**). Contour plots of some selected molecular orbitals show that the high energy occupied molecular orbitals (HOMOs) for (**1**) (β-spin) have 100% π(L) character while the β-spin low energy unoccupied molecular orbital (LOMO) have been constructed by 80% *d*π(Ni) character along with a reduced contribution of 20% π(L) character ((Supplementary Data, Fig. S3). Similarly in complex (**2**), HOMO orbitals of β-spin state have 90% π(L) character along with reduced contribution *d*π(Ni) orbital (Supplementary Data, Fig. S4). Similarly, LUMO orbitals contributed 92% π(L) character along with reduced contribution of 8% *d*π(Ni) character[35]. Spin density maps were generated to localize the electron density of the unpaired electron (Fig. 4). The spin density of the unpaired spin was distributed over 65% Ni, 5% O, 12% N, and 18% C for (**1**), and, 40% Ni, 42% N, 10% O, and 8% C for (**2**) on the coordinated atoms along with a major contribution on the nickel center.

Conclusions

The synthesis and characterization of two new mononuclear nickel(II) complexes, namely, $[Ni(HL)(L)]NO_3$ (**1**) and $[Ni(L)_2]4H_2O$ (**2**) is reported. These complexes are structurally characterized by single crystal X-ray analysis. Magnetic moments and electronic spectral studies suggest six-coordinate geometry for both the complexes. The geometry of the molecules are optimized with the DFT-B3LYP method using LANL2DZ basis sets for ligand and nickel(II). The electronic transitions determined experimentally are comparable with those obtained theoretically from TD-DFT calculations.

Supplementary Data

The X-ray crystallographic data for the structures reported herein have been deposited under CCDC no. 1507721 (**1**) and 1507726 (**2**). These data can be obtained free of charge via http://www.ccdc.cam.ac.uk/structure-summary-form the Cambridge Crystallographic Data Centre, 12 Union Road, Cambridge CB2 1EZ, UK; Email: deposit@ccdc.cam.ac.uk. Other supplementary data associated with this article are available in the electronic form at http://www.niscair.res.in/jinfo/ijca/IJCA_57A(01)44-51_SupplData.pdf.

Acknowledgement

Our grateful thanks are due to School of Chemistry, University of Hyderabad, Hyderabad, India for single crystal X-ray data collection. CDRI, Central Drug Research Institute, Lucknow, India is also thankfully acknowledged for providing analytical and spectral facilities.

References

1 Bhattacharya P, Parr J & Ross A T, *J Chem Soc Dalton Trans,* (1998) 3149.
2 Patel R N, Shukla K K, Singh A, Patel D K & Sondhiya V P, *Trans Met Chem,* 36 (2011) 179.
3 Xu C, Chen Pei-Kun, Mao Hong-yan, Shen Xiao-qing, Zhang Hong-Yun & Yu Z, *Synth React Inorg Met-Org Nano-Metal* Chem, 35 (2005) 773.
4 Murata T, Yakiyama Y, Nakasuji K & Morita Y, *Cryst Growth Des,* 10 (2010) 4898.
5 Denis P & Ventura O N, *J Mol Struct,* 537 (2001)173.
6 Song Y Z, Zhou J F, Song Y, Wei YG & Wang H, *Bioorg Med Chem Lett,* 15 (2005) 4672.
7 Jacob R & Fiscker G, *J Mol Struct,* 613 (2002) 175.
8 Jayabharathi J, Thanikachalam V & Perumal M V, *Spectrochim Acta: Part A,* 95 (2012) 614.
9 Datta A, Sheu SC, Liu P H & Huang J H, *Acta Crystallogr, Sect E*, 67 (2011)1852.
10 *SMART, SAINT, Software Reference Manual*, (Bruker AXS Inc, Madison, WI) 2000.
11 Sheldrick G M, *Acta Crystallogr,* 64A (2008) 112.
12 *APEX2, SAINT*, (Bruker, AXS Inc., Madison Wisconsin, USA) 2004.
13 Sheldrick G M, *A*cta *Crystallogr, Sect A: Fundam Crystallogr,* 46 (1990) 467.
14 Ferrugia J L, *J Appl Crystallogr,* 45 (2012) 849.
15 Spek A L, *Acta Crystallogr, Sect A: Fund Crystallogr,* 46 (1990) C34-34.
16 Becke M A D, *Phys Rev A*, 38 (1988) 3098.
17 *Gaussian 09, Revision D.01*, (Gaussian, Inc., Wallingford CT) 2013.
18 Dozer D T & Handy N C, *Phys Chem,* 2 (2000) 2117.
19 Patel R N, *Indian J Chem,* 48A (2009) 1370.
20 Geary W J, *Coord Chem Rev,* 7 (1971) 81.

21 Elber S R, Helland B J, Jacobson R A & Angilicy R J, *Inorg Chem,* 19 (1980) 175.

22 Battablia L P, Corradi A B, Antolini L, Marcotrigiano G, Menabue L & Pellacani G C, *J Am Chem Soc,*104 (1982) 2407.

23 Patel R N, Singh Y P, Singh Y, Butcher R J, Zeller M, Singh R K B & U-wang O, *J Mol Struct,* 1138 (2017) 157.

24 Mendes I C, Costa F B, De-Lima G M, Ardisson J D, Garcia-Santos I, Castineiras A & Beraldo H, *Polyhedron*, 28 (2009) 1179.

25 Matovic Z D, Miletic V D, Cendic M, Meetsma A, Vankoningsbruggen P J & Derth R J, *Inorg Chem,* 52 (2013) 1238.

26 Patel R N, Singh Y P, Singh Y & Butcher R J, *Indian J Chem,* 54A (2015) 1459.

27 Patel R N, Singh Y, Singh Y P & Butcher R J, *J Coord Chem,* 69 (2016) 2377.

28 Patel R N, Shukla K K, Singh A, Choudhary M, Patel D K, Niclo-Gutierrez J & Choquesillo-Lazarte D, *J Coord Chem,* 63 (2010) 3648.

29 Sundaraganesan N, Kalaichelvan S, Meganathan C, Dominic-Joshua B & Cornard J, *Spectrochim Acta: Part A,* 71 (2008) 898.

30 Ramalingam S, Periandy S & Mohan S, *Spectrochim Acta: Part A,* 77 (2010) 73.

31 Zhang F, Tang Y, Cao Z, Jing W, Wu Z & Chen Y, *Corr Sci,* 61 (2012) 1.

32 Barone V & Cossi M, *J Phys Chem,* 102A (1998) 1995.

33 O'Boyle N M, Tenderholt A L & Langner K M, *J Comp Chem,* 29 (2008) 839.

34 Dennington R K & Millam T, *GaussView, Version 5*, (J Semichem Inc Shawnee Mission KS), 2009.

35 Manda S, Naskar B, Modak R, Sikdar Y, Chatterjee S, Biswas S, Mondal T K, Modak D & Goswami S, *J Mol Struct*, 1088 (2015) 38.